JALS Vol.2 n.1
Journal of Applied and Laser Spectroscopy 2015

Steady-state fluorescence-phosphorescence studies of Radachlorin® kinetics and singlet oxygen formation in water

A.L. Glazov [1], I.V. Semenova [1], O.S. Vasyutinskii [1,2]

[1] *Ioffe Physical Technical Institute; 26, Polytekhnicheskaya, St.Petersburg, 194021, Russia*
[2] *St.Petersburg State Polytechnic University; 29, Polytekhnicheskaya, St.Petersburg, 195251, Russia*

Received 27/04/2015 accepted 04/05/2015

ABSTRACT

The experimental study on in vitro steady-state kinetics of Radachlorin photosensitizer fluorescence and singlet oxygen phosphorescence as a function of the photosensitizer concentration in an aqueous solution is presented. The thorough in vitro evaluation of photophysical properties of photosensitizers applied in photodynamic therapy is a prerequisite of their efficient usage in medical practice. Among other parameters the photosensitizer photobleaching is one of the important factors affecting the photodynamic therapy efficiency. The results obtained were interpreted on the basis of rate equations describing excitation and degradation of the photosensitizer molecules and singlet oxygen generation. It was demonstrated that the experimental method used allows to evaluate a bleaching rate coefficient, a diffusion coefficient, and a ratio of the absorption and fluorescence rate constants which are important photophysical parameters characterizing singlet oxygen generation. It was also observed that with an increase of the photosensitizer concentration the singlet oxygen concentration approaches an upper limit. This result can be utilized for providing optimal photosensitizer concentration and excitation light intensity for singlet oxygen generation in solutions.

1. INTRODUCTION

The rapidly advancing nowadays field of photodynamic therapy (PDT) of various diseases stimulates research activities aimed to the development and validation of novel photosensitizers (PS). Among the major factors affecting the photosensitizer efficiency are the singlet oxygen (SO) quantum yield and PS photostability. State-of-the-art technologies of infrared detectors allow monitoring of the very weak signal of SO phosphorescence at the wavelength around 1270 nm that can give direct information on SO kinetics and quantum yield in the system. Information on PS photostability can be extracted from the data on its fluorescence kinetics. Irreversible PS photobleaching may occur due to photomodification or fragmentation of the chromophore, both of these processes resulting in the decay of PS absorption and fluorescence. Note though that since fluorescence depends also on quenching its decay is not solely due to the absorption decay. That is why the combined recording of both the PS fluorescence kinetics and SO phosphorescence kinetics can provide a complete set of data on PS photostability and SO formation in the system.

Studies of PS fluorescence and SO phosphorescence kinetics are performed either in time-resolved experiments under pulsed laser excitation with the following recording of luminescence intensity decay on the microsecond scale (e.g. [1]), or in steady-state regime with CW laser excitation and data collection over long time periods of the order of minutes or even hours (e.g. [2]). Both approaches exhibit their own advantages and drawbacks.

The time-resolved approach provides direct determination of SO quantum yield from its phosphorescence lifetime. Alternatively, the fluorescence decay time depends besides the fluorophore parameters on various factors, such as pH, viscosity and refractive index of the solute as

Corresponding author: I.V. Semenova, e-mail: irina.semenova@mail.ioffe.ru
Keywords: Fluorescence, Phosphorescence, Photodynamic Therapy

well as on the quenching rate by surrounding molecules and formation of aggregates [3].

The steady-state approach allows to study the PS photodegradation using the fluorescence decay rate as a function of various parameters, such as illumination time, fluence rate or irradiation wavelength (see e.g. [4], where fluorescence decay of Photodithazine® PS was measured as a function of time and fluence rate for different irradiation wavelengths). Most of photosensitizers such as porphyrins, chlorins, phthalocyanines etc. used in the photodynamic therapy are not photostable. Almost all of them are degraded by light due to either fragmentation of macrocycles or photoproducts formation ([5]). Reversible and irreversible photobleaching effects have to be taken into account when determining photodynamic dose and photosensitizer concentration during PDT.

The properties of PSs required for successful application in PDT are listed in a variety of sources (see e.g. [6]). Briefly they are: high quantum yield of SO; selective accumulation in targeted tissues and intracellular localization in targeted cells; fast removal from the body; besides that the absorption band shifted towards the therapeutic window is highly desirable.

Radachlorin® is the patented composition of sodium salts of chlorin e6 (80%), purpurin 5 (15%) and chlorin p6 (5%). The photosensitizer is developed and produced by RadaPharma Ltd. (Moscow, Russia) [7]. It is clinically approved and is applied for fluorescent diagnostics and photodynamic therapy of malignant tumors. According to the developers Radachlorin combines high cytophototoxicity and low dark toxicity, fast and sufficiently selective accumulation in target tissues, beyond that, it is excreted from the body relatively rapidly (in 1-2 days).

The major component of Radachlorin, chlorin e6, was studied for more than 20 years and a large amount of data on its photophysics is accumulated by now (see [2, 6, 8-10] and references therein). Much less attention had been paid to Radachlorin. A majority of the papers are devoted to clinical PDT trials with this PS ([11-14]), with only a few papers considering its photophysical properties ([4]).

In Table 1 we present a summary of the available data on photophysical parameters of Radachlorin taken from various sources. The data on chlorin e6 parameters are summarized in Table 2. Table 3 presents data on SO parameters.

Absorption maxima	406 (Soret band), 506, 536, 608, 662 (Q band), nm 405, 660, 960 nm	Slightly shift with solute and pH H_2O, pH = 7.0	[7] Own measurements
Fluorescence maximum	660-668 nm 660 nm	Slightly shifts with solute and pH H_2O, pH = 7.0	[7], [14] Own measurements
Fluorescence quantum yield	0.04		[7], [14]
Interconversion quantum yield	0.96		[7]
Extinction coefficient (662 nm)	34200 $M^{-1}cm^{-1}$	In the presence of human serum albumin	[14]
Singlet oxygen quantum yield	0.52-0.62	In the presence of human serum albumin	[14]
Phosphorescence maximum	960 nm		Own measurements

Table 1. Photophysical parameters of Radachlorin

Absorption maxima □□□Soret band□ □□□Q band□	 402 nm 654 nm	pH = 7.4	[10]
Fluorescence maximum	662 nm	pH = 7.4	[10]
Fluorescence quantum yield	0.18	pH = 7.4	[10]
Lifetime of the first excited singlet state	4.3 ns	pH = 7.4	[10]
Lifetime of the first excited triplet state	2.1 □s 0.9 □s	pH = 7.4 H_2O	[10] [15]
Maximum of phosphorescence from the first excited triplet state	830 — 900 nm		[9]
Extinction coefficients: 402 nm 663 nm	 150,000 $M^{-1}cm^{-1}$ 59,000 $M^{-1}cm^{-1}$		[8]
Fluorescence quantum yield	0.18		[9]
Quantum yield of triplet formation	0.74		[9]
Singlet oxygen quantum yield	0.74		[9]

Table 2. Photophysical parameters of chlorin e6

Lifetime of the $^1\Box_g$ state	3.7 μs 0.1 μs	aqueous media biological media	[15]
Radiative lifetime of the $^1\Box_g$ state	3.3 s	H_2O	[16]
Diffusion length	$2 \cdot 10^{-5}$ cm^2s^{-1}	H_2O	[17]
Quantum yield	$4 \cdot 10^{-7}$ $9.3 \cdot 10^{-7}$	H_2O H_2O	[17] [16]

Table 3. Singlet oxygen parameters

2. Experimental Approach

The schematic of the experimental setup is shown in Figure 1. The output beam of a semiconductor laser (405 nm, 50mW) illuminated the surface of an aqueous PS solution in the experimental cell at the fluence rate 3.3 W/cm².

Two simultaneously operating measurement channels are utilized. The Radachlorin fluorescence at the spectral band centered at 660 nm was measured by the lock-in amplifier with the silicon photodiode as an input detector. The phosphorescence of singlet oxygen at about 1270 nm was detected by the cooled NIR PMT module (Hamamatsu H10330B-45). The data was accumulated by the homemade photon counter during the 5-ms period and averaged over 100 periods. Two filters were placed in front of the PMT module: the interference filter (central wavelength 1280 nm, FWHM 70 nm) and silicon filter with the short cut at approx. 1050 nm. Note that this set of filters cuts the weak photosensitizer phosphorescence at 960 nm (see Table 1). The reference frequency of 200 kHz was provided by the opto-mechanical modulator (chopper). The same

modulator could be inserted into the excitation beam path to facilitate measurements in a chopped regime. The both channels provided simultaneous time-dependent series of signals measured in chopped and non-chopped modes.

The ability to obtain simultaneous measurements of PS fluorescence and $^1O_2$ phosphorescence is expected to be valuable for assessing the relationship between PS bleaching and $^1O_2$ production. Note that dual-channel fluorescence-phosphorescence configurations have been successfully used for imaging of PS/singlet oxygen distributions in tissues even in vivo ([18, 19]).

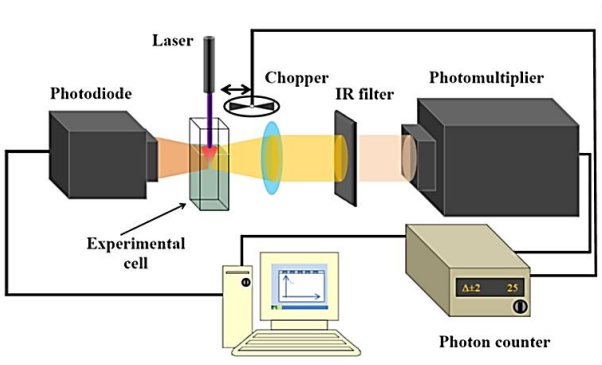

Figure 1: Basic schematic of the experimental setup.

3. Results and Discussion

3.1 Photosensitizer fluorescence kinetics

Figure 2 presents temporal decay of the fluorescence intensity of Radachlorin dissolved in water with PH = 7.0 at different concentrations. Measurements were taken in the chopped regime.

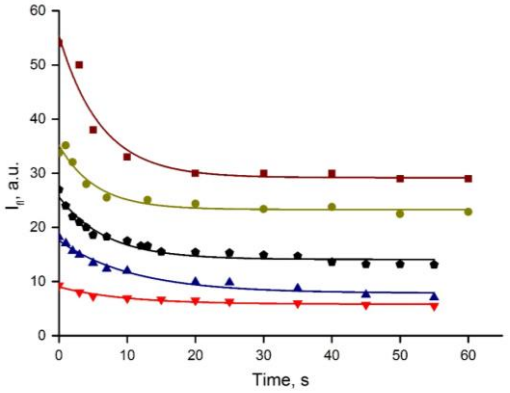

Figure 2. Radachlorin fluorescence intensity in the spectral band centered at 660 nm as a function of time. Symbols represent different Radachlorin concentrations, N_R, in water:
▼: N_R = 1.2 ·10^{15}cm^{-3}
▲: N_R = 2.3 ·10^{15}cm^{-3}
⬟: N_R = 4.5 ·10^{15}cm^{-3}
●: N_R = 9.0 ·10^{15}cm^{-3}
■: N_R =1.75 ·10^{16}cm^{-3}

The symbols in Figure 2 represent our experimental data and solid curves are fit. Different curves in this figure relate to different photosensitizer concentrations, N_R. As can be seen from Figure 2 under the condition of continuous wave exposure the fluorescence intensities exhibit maxima at the beginning of laser irradiation (t=0) and then a slow decrease steadily approaching a plateau at long times. The physical reason of the decrease is the dye photobleaching inside the interaction volume which is a cylinder with a base equal to the laser beam cross section S ≈ 1.5 mm² and a height h of about 5 mm. The plateaus correspond to an equilibrium between the dye molecules bleached inside the interaction volume and those coming into the interaction volume from the surrounding solution due to diffusion flux.

All fitting curves in Figure 2 can be described by a simple exponential expression:

$$I_{fl} = C_1 e^{-At} + C_2, \quad (1)$$

where C_1, A, and C_2 are fitting parameters.

The fitting parameters in eq. (1) determined from the experimental data in Figure 2 are presented in Table 3.

N_R, 10^{15} cm^{-3}	C_1	C_2	A
1.2	3.2 (0.1)	5.8 (0.1)	0.10 (0.01)
2.3	9.7 (0.5)	7.9 (0.4)	0.09 (0.02)
4.5	11.6 (0.6)	14.1(0.3)	0.15 (0.02)
9.0	11.9 (1.0)	23.2 (0.5)	0.19 (0.04)
17.5	26.2 (2.5)	29.2 (1.2)	0.16 (0.04)

Table 3. Fitting parameter values determined from Figure 2.

As can be shown if the laser light absorption by the dye molecules is weak the parameters C_1, A, and C_2 in eq. (1) can be presented in terms of the clear physical quantities describing photobleaching of the photosensitizer molecules and molecular diffusion through the interaction volume interface. The relationship between the fitting parameter values and physical quantities can be approximated in the form:

$$C_1 \approx \gamma \frac{N_R V f_{ab}}{f_{fl}} \left(1 - \frac{D_m}{A}\right), \quad (2)$$

$$C_2 \approx \gamma \frac{N_R V f_{ab}}{f_{fl}} \frac{D_m}{A}, \quad (3)$$

$$A \approx \frac{\alpha f_{ab}}{f_{fl}} + D_m, \quad (4)$$

where $D_m = \frac{D}{\pi}\left(\frac{1}{r_0^2} + \frac{1}{z_0^2}\right)$ is a modified diffusion coefficient, D is a diffusion coefficient, r_0 and z_0 are dimensions of the cylindrical absorption volume V, f_{ab} and f_{fl} are the dye molecule absorption and fluorescence rate constants, N_R is the dye concentration outside the absorption volume indicated in the caption to Figure 2, γ is the fluorescence detection efficiency, and α is a bleaching rate coefficient describing a relative number of the dye molecules destroyed by laser light per second.

The fluorescence rate constant f_{fl} in eqs. (2)-(4) is directly related to the fluorescence lifetime: $f_{fl} = 1/\tau_{fl}$ and the absorption rate constant f_{ab} is proportional to the laser light intensity I_o:

$f_{ab} = I_o\,\sigma\,/\,(S\,h\nu)$, where σ is the dye molecule absorption cross section, S is the laser beam cross section, and $h\nu$ is the laser photon energy.

The weak absorption approximation in eqs. (2)-(4) is valid for the three lowest curves in Figure 2. These data, eqs. (2)-(4) and the fitting parameter values in Table 3 can be used for determination of the physical quantities describing the dye molecules evolution in experiments.

3.2 Singlet oxygen phosphorescence kinetics

Singlet oxygen phosphorescence intensity at 1270 nm as a function of time is presented in Figure 3. Measurements were taken in the non-chopped regime. Different curves in this figure relate to different PS concentrations, N_R, in agreement with Figure 2. As can be seen from Figure 3 the phosphorescence intensity first rises sharply during about a second after the beginning of irradiation (t=0) and then remains almost constant at relatively high PS concentrations, or decreases slowly steadily approaching a plateau at relatively low PS concentrations (three low-lying curves in Figure 3). As can be seen in Figure 3 at relatively low PS concentrations the maximum phosphorescence intensity increases with N_R, however at relatively high PS concentrations the maximum phosphorescence intensity approaches the limit of about 50 a.u. which does not depend on N_R.

The phosphorescence intensity in Figure 3 is directly proportional to the SO concentration, N_{SO}, which evolves in time according to the following rate equation:

$$\frac{\partial N_{SO}}{\partial t} = \gamma_{SO} N_{RT} - \frac{N_{SO}}{\tau_q}, \qquad (5)$$

where N_{RT} is the concentration of excited triplet PS molecules, γ_{SO} is the rate constant describing SO generation due to collisions between ground state oxygen molecules and the excited triplet PS molecules: $\gamma_{SO} = N_O < v\sigma_{SO} >$, τ_q is the SO lifetime describing SO quenching due to collisions with PS molecules and with water molecules:

$$\tau_q^{-1} = N_R < v\sigma_R > + N_{RT} < v\sigma_{RT} > + N_w < v\sigma_w >, \qquad (6)$$

where N_w and σ_w are, respectively, water molecules concentration and SO quenching cross section due to collisions with water molecules.

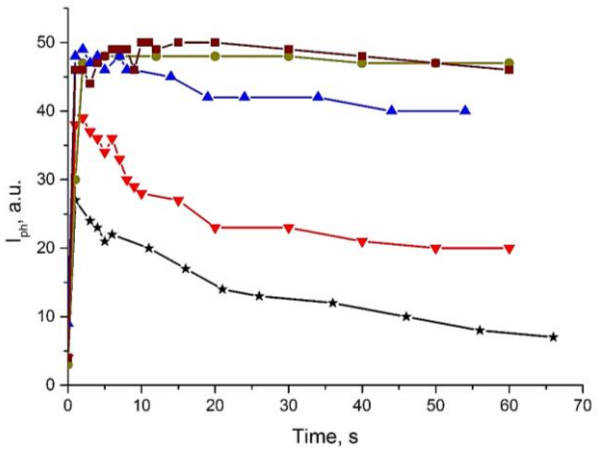

Figure 3: Singlet oxygen phosphorescence intensity at 1270 nm as function of time.
Different symbols represent different Radachlorin concentrations, N_R:
★: N_R = 6.0 ·10¹⁴cm⁻³
▼: N_R = 1.2 ·10¹⁵cm⁻³
▲: N_R = 2.3 ·10¹⁵cm⁻³
●: N_R = 9.0 ·10¹⁵cm⁻³
■: N_R = 1.75 ·10¹⁶cm⁻³

The relatively sharp rise of the phosphorescence intensity in the vicinity of t=0 is described by the first term in the *rhs* in eq. (5). Note that the phosphorescence intensities in Figure 3 were recorded in a single photon counting regime and then averaged over the time of about 0.5 s. Therefore, the slope of lines in the vicinity of the origin does not represent the dynamics of a real photochemical process, but just a result of the signal averaging.
Having in mind a relatively slow variation of the SO phosphorescence intensity in Figure 3, SO concentration at time t > 1 s can be presented as a stationary solution of eq. (5):

$$N_{SO}(t) = \gamma_{SO}\tau_q(t)N_{RT}(t)\,, \qquad (7)$$

where N_R in eq. (6) and N_{RT} in eq. (7) decrease in time due to photobleaching of the photosensitizer molecules.

As can be seen from eqs. (6) and (7) at low PS concentrations when quenching of SO due to interaction with water molecules is a major contribution in eq. (6) the SO concentration is proportional to the excited triplet PS molecule concentration which decreases slowly steadily approaching a plateau (see three low-lying curves in Figure 3).
At high PS concentration when quenching of SO due to interaction with PS molecules is a major contribution in eq. (6) the SO concentration practically does not depend on N_R (see two higher-lying curves in Figure 3). Therefore, the simple theoretical model used is in a good qualitative agreement with the experimental data.

CONCLUSIONS

The paper presents in vitro steady-state experiments on simultaneous recording of Radachlorin photosensitizer fluorescence kinetics and singlet oxygen phosphorescence kinetics induced in the PS aqueous solution by CW laser radiation in the PS Soret absorption band. The results obtained were interpreted on the basis of a set of rate equations describing excitation and degradation of the photosensitizer molecules and singlet oxygen generation. As shown, the photosensitizer fluorescence kinetics obeys a simple exponential law with the intensity approximately proportional to the photosensitizer concentration. This result is interpreted in terms of a competition between the photosensitizer bleaching and diffusion flux into the interaction volume from the surrounding solution. The singlet oxygen phosphorescence intensity demonstrated a well defined upper limit achieved with the increase of photosensitizer concentration which was interpreted as a result of quenching collisions between the singlet oxygen and the photosensitizer molecules. It was shown that the experimental method used allows to evaluate important photophysical parameters and to determine optimal values of photosensitizer concentration and excitation light intensity for efficient generation of singlet oxygen in the system.

REFERENCES

[1] R. Dedic, A. Svoboda, J. Psencık, J. Hala, "Phosphorescence of singlet oxygen and meso-tetra (4-sulfonatophenyl)porphin: time and spectral resolved study", *Journal of Molecular Structure*, **651–653C**, pp. 301–304, (2003).

[2] J. Ferreira, P.F.C. Menezes, C. Kurachi, C. Sibata, R.R. Allison, V.S. Bagnato, "Photostability of different chlorine photosensitizers", *Laser Phys. Lett.*, **5**, 2, pp. 156-161, (2008).

[3] K. Suhling, P.M.W. French, D. Phillips, "Time-resolved fluorescence microscopy", *Photochem. Photobiol. Sci.*, **4**, pp. 13–22, (2005).

[4] F. Vargas, Y. Díaz, V. Yartsev, A. Marcano, A. Lappa, "Photophysical properties of novel PDT photosensitizer Radachlorin in different media", *Ciencia*, **12** (1), pp. 70-77, (2004).

[5] A. Juzeniene, Q. Peng, J. Moana, "Milestones in the development of photodynamic therapy and fluorescence diagnosis", *Photochem. Photobiol. Sci.*, **6**, pp. 1234–1245, (2007).

[6] *Photosensitizers in Medicine, Environment, and Security. Tebello Nyokong, Vefa Ahsen* (Eds.), Springer, p. 655, (2012).

[7] http://www.radapharma.ru/radahlorin.php

[8] J.F. Lovell, T.W.B Liu, J.Chen, G. Zheng, "Activatable Photosensitizers for Imaging and Therapy." *Chem. Rev.,* **110**, pp. 2839–2857, (2010).

[9] A.P. Losev, I.N. Nichiporovich, I.N. Zhuravkin, E.I. Zhavrid, "The energetics of chiorins as potent photosensitizers of PDT", *Proc. SPIE*, Vol. 2924, 40-44, (1996).

[10] H.A. Isakau, M.V. Parkhats, V.N. Knyukshto, B.M. Dzhagarov, E.P. Petrov, P.T. Petrov, "Toward understanding the high PDT efficacy of chlorin e6–polyvinylpyrrolidone formulations: Photophysical and molecular aspects of photosensitizer–polymer interaction in vitro", *Journal of Photochemistry and Photobiology B: Biology*, **92**, pp. 165–174, (2008).

[11] S. Douillard, D. Olivier, T. Patrice, "*In vitro* and *in vivo* evaluation of Radachlorin® sensitizer for photodynamic therapy", *Photochem. Photobiol. Sci.*, **8**, pp. 405–413, (2009).

[12] S. Douillard, I. Lhommeau, D. Olivier, T Patrice, "In vitro evaluation of Radachlorin® sensitizer for photodynamic therapy", *Journal of Photochemistry and Photobiology B: Biology*, **98**, pp. 128–137, (2010).

[13] A.B. Uzdensky, O.Y. Dergacheva, A.A. Zhavoronkova, A.V. Reshetnikov, G.V. Ponomarev, "Photodynamic effect of novel chlorin e6 derivatives on a single nerve cell", *Life Sciences*, **74**, pp. 2185 – 2197 (2004).

[14] V.A. Privalov, A.V. Lappa, E.V. Kochneva, "Five Years' Experience of Photodynamic Therapy with New Chlorin Photosensitizer", *Proc. SPIE*, Vol. 5863, pp. 186-198, (2005).

[15] S. Lee, L. Zhu, A.M. Minhaj, M.F. Hinds, D.H. Vu, D.I. Rosen, S.J. Davis, T. Hasan, "Pulsed diode laser-based monitor for singlet molecular oxygen", *J Biomed Opt.*, **13** (3), 034010 (2008).

[16] A.P. Losev, I.M. Byteva, G.P. Gurinovich, "Singlet oxygen luminescence quantum yields in organic solvents and water", *Chem. Phys. Lett.*, Vol. 143, 2, pp. 127-129, (1988).

[17] A.A. Krasnovsky, "Singlet Molecular Oxygen in Photobiochemical Systems: IR Phosphorescence Studies", *Membr. Cell Biol.*, Vol. 12 (5), pp. 665-690 (1998).

[18] S. Lee, M.E. Isabelle, K.L. Gabally-Kinney, B.W. Pogue, S.J. Davis, "Dual-channel imaging system for singlet oxygen and

photosinsitizer for PDT", *Biomedical Optics Express*, **2**, 5, pp. 1233-1242 (2011).

[19] V. Vyklicky, R. Dedic, N. Curkaniuk, J. Hala, "Spectral-and time-resolved phosphorescence of photosensitizers and singlet oxygen: From in vitro towards in vivo", *Journal of Luminescence*, **143**, pp. 729–733 (2013).